

# Lumazine Synthase from *Candida albicans* as an Anti-fungal Target Enzyme

## STRUCTURAL AND BIOCHEMICAL BASIS FOR DRUG DESIGN\*

Received for publication, February 27, 2007, and in revised form, April 18, 2007. Published, JBC Papers in Press, April 18, 2007, DOI 10.1074/jbc.M701724200

Ekaterina Morgunova<sup>†1</sup>, Sabine Saller<sup>§</sup>, Ilka Haase<sup>¶</sup>, Mark Cushman<sup>||</sup>, Adelbert Bacher<sup>§</sup>, Markus Fischer<sup>¶</sup>, and Rudolf Ladenstein<sup>‡</sup>

From the <sup>‡</sup>Karolinska Institutet, NOVUM, Centre for Structural Biochemistry, Hälsovägen 7-9, S-14157 Huddinge, Sweden, the <sup>§</sup>Lehrstuhl für Organische Chemie und Biochemie, Technische Universität München, Lichtenbergstrasse 4, D-85747 Garching, Germany, the <sup>¶</sup>Institut für Biochemie und Lebensmittelchemie, Abteilung Lebensmittelchemie, Universität Hamburg, Grindelallee 117, 20146 Hamburg, Germany, and the <sup>||</sup>Department of Medicinal Chemistry and Molecular Pharmacology, School of Pharmacy and Pharmaceutical Sciences, and the Purdue Cancer Center, Purdue University, West Lafayette, Indiana 47907

Lumazine synthase is an enzyme involved in riboflavin biosynthesis in many plants and microorganisms, including numerous human pathogens. The fact that the enzymes of the riboflavin biosynthesis pathway are not present in the human or animal host makes them potential targets for anti-infective agents. The crystal structure of lumazine synthase from *Candida albicans* was solved by molecular replacement and refined at 2.5-Å resolution. The results of crystallographic investigations and sedimentation equilibrium experiments clearly indicated the presence of pentameric assemblies of the enzyme either in crystals or in solution. Isothermal titration calorimetry measurements of the binding reactions of four different inhibitors revealed high affinity for all four compounds with binding constants in the micromolar range. Structural comparison with previously determined structures of the enzyme-ligand complexes of other orthologues allowed modeling of the binding of four different inhibitors into the active site of lumazine synthase from *Candida albicans*.

Among human fungal pathogens, *Candida albicans* plays a dominant role. This opportunistic yeast is responsible for ~8% of all hospital-acquired fungal infections and poses a serious health risk to immunocompromised individuals, including AIDS patients, cancer patients, diabetics, newborns, and the elderly (1). The remarkable ability to survive and proliferate in a radically changing environment has placed *C. albicans* as the fifth leading cause of microbial infections in hospital settings (2). Although several anti-fungal agents, such as amphotericin B and the azole class of drugs, are currently available (3, 4), there is clearly a critical need for the development of new specific

anti-fungal agents. Because bacteria and fungi (5–7) are not able to incorporate vitamin B<sub>2</sub> (riboflavin) from the environment, they are absolutely dependent on endogenous biosynthesis of this cofactor. In contrast, humans lack riboflavin biosynthesis enzymes and must obtain the vitamin from dietary sources. Therefore, the enzymes of the riboflavin biosynthetic pathway represent potential targets for antibiotic agents.

Despite the fact that studies of riboflavin biosynthesis have a long and successful history, the three-dimensional structure of only one *C. albicans* enzyme involved in riboflavin biosynthesis is available in the Protein Data Bank (8). 3,4-Dihydroxy-2-butanone 4-phosphate synthase catalyzes the formation of 3,4-dihydroxy-2-butanone 4-phosphate (2), one of two substrates needed for the synthesis of 6,7-dimethyl-8-(D-ribityl)lumazine (3). In the following step one riboflavin molecule 4 is synthesized from two molecules of 3 (Fig. 1). Condensation reaction of 2 with the second substrate 5-amino-6-ribitylamino-2,4-(1*H*,3*H*)-pyrimidinedione (1) is catalyzed by lumazine synthase (LS).<sup>2</sup> Finally, the dismutation reaction of two molecules of 3 resulting in one molecule of riboflavin and one molecule 1 is catalyzed by riboflavin synthase (RS).

LS, which catalyzes the penultimate step in riboflavin biosynthesis pathway, is the target of our interest. This enzyme has been observed in pentameric assembly form in *Saccharomyces cerevisiae*, *Schizosaccharomyces pombe*, *Magnaporthe grisea*, and *Mycobacterium tuberculosis*, as dimers of pentamers in *Brucella abortus* and as icosahedral capsids consisting of 60 subunits (12 pentamers) in *Bacillus subtilis*, *Aquifex aeolicus*, and *Spinacia oleracea* (9–16). The comparison of known three-dimensional structures of LS from different species showed a homologous flavodoxin-like fold regardless of the quaternary structures of the enzymes. The folding pattern comprises a central four-stranded β-sheet flanked on both sides by two and three α-helices, respectively. In all LS structures, the topologically equivalent active sites are located at the interfaces between

\* This work was supported by the Swedish Research Council (Vetenskapsrådet) (Project 621-2001-3195), National Institutes of Health Grant GM 51469, the Hans Fischer Gesellschaft e.V., and the Fonds der Chemischen Industrie. The costs of publication of this article were defrayed in part by the payment of page charges. This article must therefore be hereby marked "advertisement" in accordance with 18 U.S.C. Section 1734 solely to indicate this fact.

The atomic coordinates and structure factors (code 2JFB) have been deposited in the Protein Data Bank, Research Collaboratory for Structural Bioinformatics, Rutgers University, New Brunswick, NJ (<http://www.rcsb.org/>).

<sup>†</sup> To whom correspondence should be addressed. Tel.: 46-8-608-9177; Fax: 46-8-608-9290; E-mail: katja.morgunova@biosci.ki.se.

<sup>2</sup> The abbreviations used are: LS, lumazine synthase; CALS, *C. albicans* lumazine synthase; RS, riboflavin synthase; MbtLS, *M. tuberculosis* lumazine synthase; **TS13**, 1,3,7-trihydro-9-D-ribityl-2,4,8-purinetrione-7-yl; **TS44**, 3-(1,3-dihydro-9-D-ribityl-2,4,8-purinetrione-7-yl)propane 1-phosphate; **GJ43**, 4-(6,7(5*H*,8*H*)-dioxo-8-D-ribityllumazin-5-yl)butane 1-phosphate; **JC33**, [4-(6-chloro-2,4-dioxo-1,2,3,4-tetrahydropyrimidin-5-yl)butyl] phosphate.

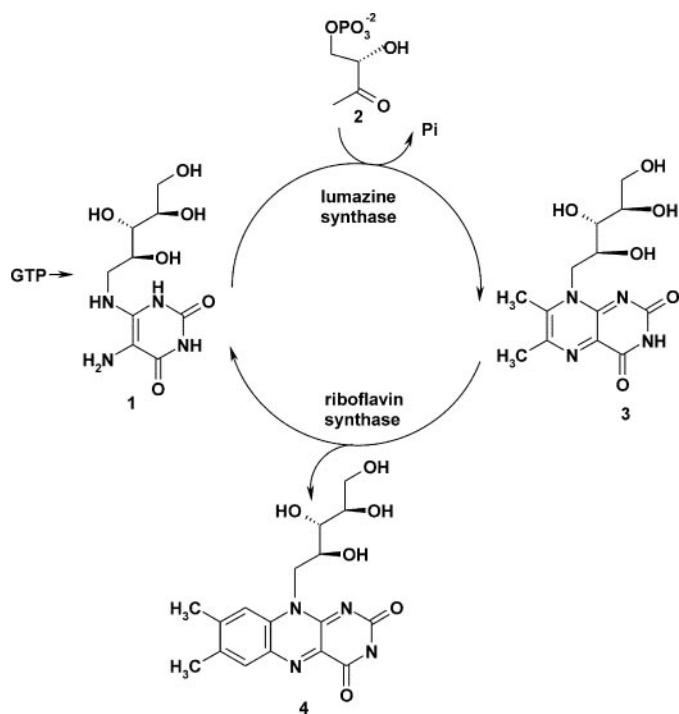


FIGURE 1. Terminal reactions in the pathway of riboflavin biosynthesis. **1**, 5-amino-6-ribitylamino-2,4(1H,3H)-pyrimidinedione; **2**, 3,4-dihydroxy-2-butanone 4-phosphate; **3**, 6,7-dimethyl-8-ribityl-lumazine; and **4**, riboflavin.

adjacent subunits in the pentamers. The binding sites of the two lumazine synthase substrates have been identified by crystallography of complexes formed between the enzyme and metabolically stable substrate, intermediate, and product analogues.

Formation of lumazine **3** consists of the following steps: substrate binding, nucleophilic attack, formation of a Schiff base intermediate, phosphate elimination, and ring closure (17). All known inhibitors of LS can be considered as potential lead compounds for the design of therapeutically useful antibiotics and anti-fungal drugs. At present the kinetic inhibition constants together with the experimentally determined complex structures with several substrate analogues, such as 5-nitroso-6-ribitylamino-2,4(1H,3H)-pyrimidinedione (11, 18), 5-nitro-6-ribitylamino-2,4(1H,3H)-pyrimidinedione (10, 19), and 5-(6-D-ribitylamino-2,4(1H,3H)-pyrimidinedione-5-yl)1-pentylphosphonic acid (9, 18), as well as the product analogues 6,7(5H,8H)-dioxo-8-ribityllumazine and 6-methyl-7(8H)-oxo-8-ribityllumazine (18), are available. Recently, a new series of compounds based on the aromatic purinetrione system and the ribityllumazinedione system bearing alkyl phosphate chains was designed by Cushman *et al.* (20, 21). In the present report we describe the three-dimensional structure of lumazine synthase from the fungal pathogen *C. albicans*, the binding analysis of four inhibitors by isothermal titration calorimetry and the docking of those compounds into the CALS active site.

## EXPERIMENTAL PROCEDURES

**Materials**—5-Amino-6-ribitylamino-2,4(1H,3H)-pyrimidinedione was freshly prepared from 5-nitro-6-ribitylamino-2,4(1H,3H)-pyrimidinedione (22, 23) by catalytic hydrogenation (24). Ribulose 5-phosphate was purchased from Sigma-Aldrich Chemie GmbH, Munich, Germany, and converted to (S)-3,4-

TABLE 1

### Bacterial strains and plasmids used in this study

Strain/plasmid	Relevant characteristics	Source
<i>E. coli</i> strains		
XL1-Blue	recA1, endA1, gyrA96, thi-1, hsdR17, supE44, relA1, lac[F', proAB, lacI <sup>q</sup> ZΔM15, Tn10(tet <sup>r</sup> )]	27
M15[pREP4]	lac, ara, gal, mtl, recA <sup>+</sup> , uvr <sup>+</sup> , Str <sup>R</sup> , (pREP4:Kan <sup>R</sup> , lacI)	28
Expression plasmids		
pNCO113	<i>E. coli</i> expression vector	28
pNCO-CARIB4	pNCO113 expressing the gene encoding lumazine synthase of <i>C. albicans</i>	This study

dihydroxy-2-butanone 4-phosphate (**2**) by the catalytic action of recombinant *Escherichia coli* (S)-3,4-dihydroxy-2-butanone 4-phosphate synthase.

Restriction enzymes and T4 DNA ligase were from New England Biolabs. EXT DNA polymerase and *Taq* polymerase were from Finnzymes (Epsou, Finland). Oligonucleotides were synthesized by Thermo Electron GmbH (Ulm, Germany). DNA fragments were purified with the CP-Kit, Gel Extraction Kit, or Miniprep Kits from Peqlab (Erlangen, Germany). Genomic DNA of *C. albicans* was obtained from the American Type Culture Collection (ATCC No. 10231D). Recombinant *E. coli* 3,4-dihydroxy-2-butanone 4-phosphate synthase (25) was prepared by published procedures.

**Enzyme Assay**—The assay method for lumazine synthase was performed as described earlier (26).

**Strains, Plasmids, and Proteins**—Bacterial strains and plasmids used in this study are summarized in Table 1.

**Cloning**—The putative gene (*orf 19.410.3*) encoding the lumazine synthase of *C. albicans* was amplified by PCR using *C. albicans* chromosomal DNA as template and the oligonucleotides CAR4-1 (5'-gttaaagggttaggagaagttgatcaaaaatcagatggtccaaattaagaattggtattcttc-3') and CAR4-HindIII (5'-tattattataagc-ttaattgaattagtgccatttc-3') as primers. The resulting fragment served as template for a second PCR using the oligonucleotides CAR4-Rbs-EcoRI (5'-ataatagaattcattaaaggagaaataaccatggc-tgtaaagggttaggagaagttgatc-3') and CAR4-HindIII as primers. The amplificate (541 bp) was digested with EcoRI and HindIII and ligated into the expression vector pNCO113. The resulting plasmid designated pNCO-CARIB4 was transformed into *E. coli* XL1-Blue cells by published procedures (27). Transformants were selected on LB agar plates supplemented with ampicillin (170 mg liter<sup>-1</sup>). The plasmid was re-isolated and transformed into *E. coli* M15 [pREP4] cells (28) carrying the pREP4 repressor plasmid for the overexpression of lac repressor protein. Kanamycin (15 mg liter<sup>-1</sup>) and ampicillin (170 mg liter<sup>-1</sup>) were added to secure the presence of both plasmids in the host strain.

**Culturing**—Recombinant *E. coli* strains were grown in Luria-Bertani broth containing ampicillin (170 mg liter<sup>-1</sup>) and kanamycin (15 mg liter<sup>-1</sup>) as required. Cultures were incubated at 37 °C with shaking. At an optical density of 0.7 (600 nm), isopropyl 1-thio-β-D-galactopyranoside was added to a final concentration of 2 mM, and the cultures were incubated for 5 h at 37 °C with shaking. The cells were harvested by centrifugation, washed with 0.9% (w/v) sodium chloride, and stored at -20 °C.

**Purification**—All purification steps were performed at 4 °C. Frozen cell mass (6 g) was thawed in 30 ml of 20 mM potassium phosphate, pH 7.0 (buffer A). The suspension was subjected to treatment with a French Press and was then centrifuged. The supernatant was passed through a column of Q-Sepharose (5 × 10 cm, Amersham Biosciences) pre-equilibrated with buffer A (flow rate: 2 ml × min<sup>-1</sup>). The column was washed with 100 ml of buffer A and developed with a linear gradient of 0 to 1.0 M potassium phosphate, pH 7.0, in a total volume of 900 ml. Fractions were combined, concentrated by ultrafiltration, and dialyzed against 100 mM potassium phosphate, pH 7.0 (buffer B, total volume, 6 ml). The solution was passed through a column of Superdex 200 (2.6 × 60 cm, Amersham Biosciences), pre-equilibrated with buffer B (flow rate, 3 ml min<sup>-1</sup>). The column was developed with buffer B. The enzyme was eluted at 196 ml. Fractions were combined and concentrated by ultrafiltration. According to SDS-PAGE, the protein sample contained <3% impurities.

**Analytical Ultracentrifugation**—Experiments were performed with an analytical ultracentrifuge Optima XL-A from Beckman Instruments (Palo Alto, CA) equipped with absorbance optics. Aluminum double sector cells equipped with quartz windows were used throughout. Protein concentration was monitored photometrically at 280 nm.

Sedimentation equilibrium experiments were performed with solutions containing 100 mM potassium phosphate, pH 7.0, and 1.8 mg of protein per milliliter at 10,000 rpm (Beckman AN-60Ti) and 4 °C. Boundary sedimentation experiments were performed at 59,000 rpm and 20 °C using a solution containing 100 mM potassium phosphate, pH 7.0, and 6.8 mg of protein per milliliter. The partial specific volume was estimated from the amino acid composition yielding a value of 0.76 ml/g (29).

**Miscellaneous**—DNA was sequenced using the method of Sanger (30) by custom sequencing service of GATC Biotech (Konstanz, Germany). N-terminal protein sequencing was performed by the automated Edman method using a 471A Protein Sequencer (PerkinElmer Life Sciences). Protein concentration was determined by using published procedures (31). SDS-PAGE using 16% polyacrylamide gels was performed according to Laemmli with molecular mass standards provided by Sigma (32).

**Crystallization**—CALS was crystallized in sitting drops by vapor diffusion. Droplets (1 μl) containing protein solution at a concentration of 7 mg/ml in 50 mM potassium phosphate at pH 7.0 were mixed with 1 μl of the reservoir solution containing 100 mM Tris-HCl, pH 7.4, 18.4% of polyethylene glycol 6000, 0.2 M potassium acetate, 40 mM dithiothreitol, and 6% (±)-2-methyl-2,4-pentanediol. Small crystals appeared after 1–2 days. After 2–3 weeks of equilibration of the drops against the reservoir solution, those crystals grew to a size of 0.4 × 0.3 × 0.2 mm. Crystals were of sufficient quality for x-ray data collection.

**Data Collection**—An x-ray intensity data set was collected at a wavelength of 0.85 Å and an oscillation range of 1° on an MAR Research 345 Image plate detector system (Deutsches Elektronen-Synchrotron (DESY) beamline BW7B at the EMBL Outstation, Hamburg, Germany) at 100 K from a single crystal using the reservoir solution as a cryoprotectant. Data collection strategy was optimized with the program BEST (33). Space group and cell parameters were determined using the auto-

**TABLE 2**  
Data collection and refinement statistics

<b>Data collection</b>	
Resolution limit (Å)	14.9–2.5
Number of observed reflections	465,237
Number of unique reflections	94,547
Highest resolution shell (Å)	2.55–2.51
Completeness overall (%)	99.8
Completeness of highest resolution shell (%)	99.9
Overall <i>I</i> /σ	15
Last shell <i>I</i> /σ	2
<i>R</i> <sub>sym</sub> overall (%) <sup>a</sup>	7.6
<i>R</i> <sub>sym</sub> highest resolution shell (%)	56.7
<b>Refinement</b>	
Non-hydrogen protein atoms	17,928
Non-hydrogen ion atoms	75
Solvent molecules	754
Resolution range (Å)	14.97–2.5
<i>R</i> <sub>cryst</sub> overall (%) <sup>b</sup>	21.04
<i>R</i> <sub>free</sub> (%) <sup>c</sup>	26.04
<b>Ramachandran plot</b>	
Most favorable regions (%)	93.3
Allowed regions (%)	6.3
Generously allowed regions (%)	0.5
<b>r.m.s. S.D.</b>	
Bond lengths (Å)	0.006
Bond angles (°)	0.89
<b>Average B-factors/S.D. (Å<sup>2</sup>)</b>	
	35.87

<sup>a</sup>  $R_{\text{sym}} = \sum_i |I_i - \langle I_i \rangle| / \sum_i \langle I_i \rangle$ , where  $I_i$  is scaled intensity of the  $i$ th observation, and  $\langle I_i \rangle$  is the mean intensity for that reflection.

<sup>b</sup>  $R_{\text{cryst}} = \sum_{\text{hkl}} |F_{\text{obs}}| - |F_{\text{calc}}| / \sum_{\text{hkl}} |F_{\text{obs}}|$ .

<sup>c</sup>  $R_{\text{free}}$  is the cross-validation  $R$ -factor computed for the test set of 5% of unique reflections.

indexing routine in DENZO (34) and have been checked with pseudo precession images generated with the program Pattern (35). X-ray data were evaluated and scaled with programs DENZO and SCALEPACK (34). The crystals belonged to the trigonal system, space group P3<sub>1</sub>21 with cell dimensions:  $a = b = 128.6$  Å,  $c = 284.9$  Å,  $\alpha = \beta = 90^\circ$ ,  $\gamma = 120^\circ$ . Statistics of the data collection are given in Table 2.

**Structure Determination**—The structure was solved by molecular replacement using the program MOLREP as implemented in CCP4 (36) with the structure of the *S. cerevisiae* LS (PDB ID: 1EJB) as a Patterson search model. The sequence alignment of CALS with *S. cerevisiae* LS, performed with ClustalW (37), revealed a sequence identity of 72.4% (Fig. 2). The asymmetric unit was found to contain three pentamers with a corresponding Matthews coefficient of 2.5 Å<sup>3</sup>/Da and 50.5% solvent content (38).

**Refinement**—The initial model consisting of three pentamers was subjected to rigid body refinement with CNS (39). Solvent flattening, histogram matching, and 5-fold non-crystallographic averaging were applied to the initial electron density with the program DM as implemented in the CCP4 package (36). The mask covering one subunit was calculated with NCS-MASK (36), and the non-crystallographic symmetry operators were improved after every cycle of averaging. This procedure dramatically improved the quality of the electron density map and allowed building of almost all residues that had been replaced by alanine in the original model.

Further refinement using the TLS option and model building was carried out with the program REFMAC5 (36) and O (40), respectively. The progress of refinement was monitored by the free  $R$ -factor with 5% of the data put aside from the calculations. The solvent molecules were added with the help of ARP/WARP

## Lumazine Synthase from *C. albicans*

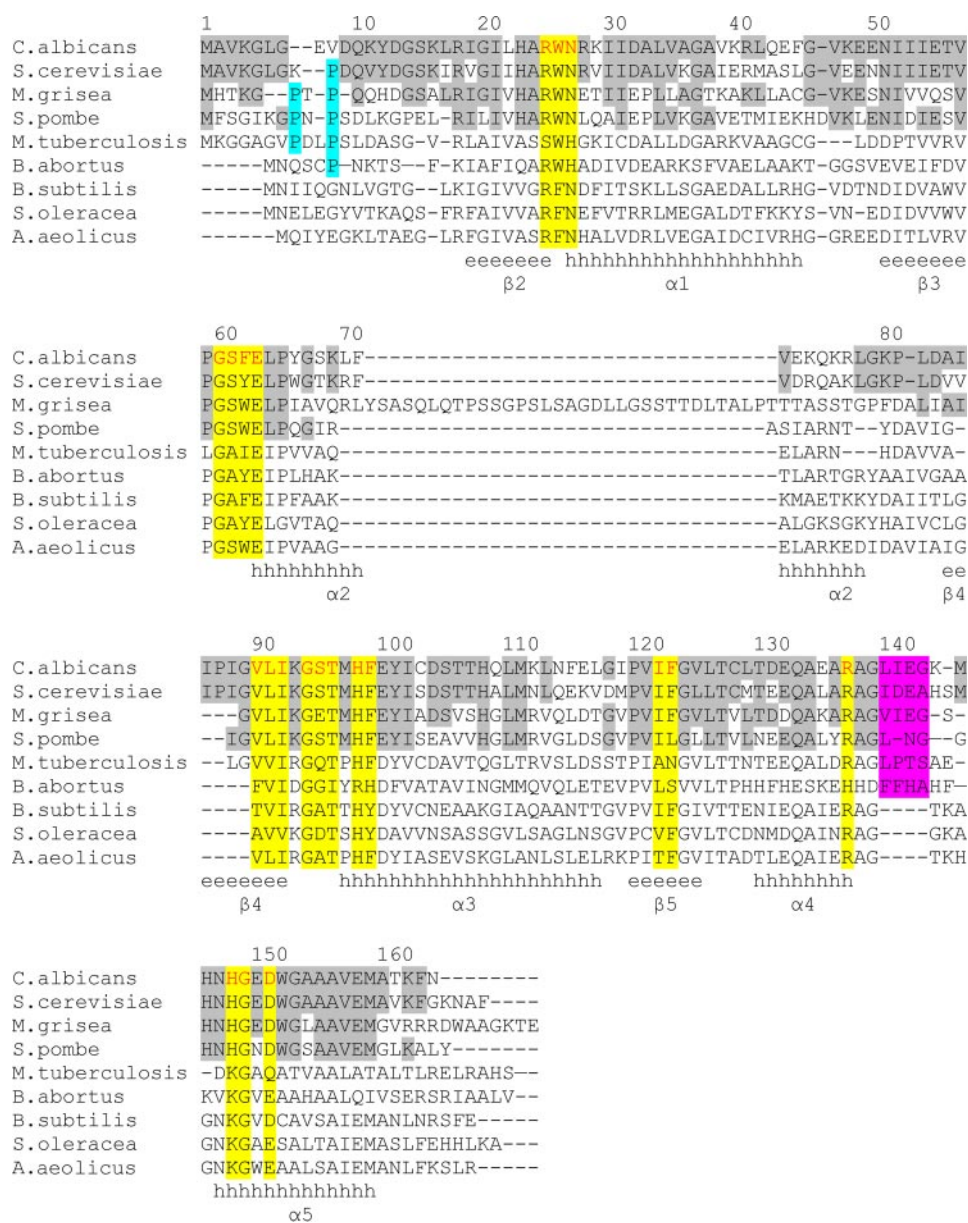


**FIGURE 2. Multiple sequence alignment of lumazine synthases with known three-dimensional structures.** The numbering above the alignment corresponds to the enzyme from *C. albicans*. Secondary structure elements are shown below the sequences as they are found in CALS. The residues conserved among fungal lumazine synthases are shown in gray. The residues involved in formation of the active site are shown in red for CALS and highlighted yellow for other LSs; putative residues, which may prevent the icosahedral assembly, are shown in magenta, the proline residues belonging to the N-terminal sequence are highlighted in cyan. Sequence alignment was performed with ClustalW (37).

program as implemented in the CCP4 package. In addition to 15 CALS subunits, 15 phosphate ions, a total of 754 water molecules and 3 ( $\pm$ )-2-methyl-2,4-pentandiol molecules were built into the  $|F_o| - |F_c|$  map during several cycles of ARP/WARP, REFMAC5 refinement, and manual rebuilding with O. Values of the final  $R_{\text{crist}}$  and  $R_{\text{free}}$  are 21.5% and 25.8%, respectively. Details of the refinement statistics are presented in Table 2.

**Inhibitors**—1,3,7-Trihydro-9-D-ribityl-2,4,8-purinetrione (TS13), 3-(1,3-dihydro-9-D-ribityl-2,4,8-purinetrione-7-yl)propane 1-phosphate (TS44), 4-(6,7(5*H*,8*H*-dioxo-8-D-ribityllumazine-5-yl)butane 1-phosphate (GJ43), and 4-(6-chloro-2,4-dioxo-

1,2,3,4-tetrahydropyrimidine-5-yl)-butyl (JC33) were prepared as described elsewhere (20, 21).

**Isothermal Titration Calorimetry**—Calorimetric measurements for binding analysis of each inhibitor were carried out by using a VP-ITC MicroCalorimeter (MicroCal, Inc., Northampton, MA). The reference cell was filled with water, and the instrument was calibrated using standard electrical pulses. All solutions were carefully degassed by stirring under vacuum before use. Binding isotherms of all ligands were measured by direct titration. A solution of CALS (0.015–0.025 mM) in 50 mM potassium-phosphate buffer at pH 7.08 in a total volume of 1.451 ml was titrated at 30 °C with 25 identical 3- $\mu$ l injections at 3-min intervals. The syringe was filled with 1.4–2.4 mM inhibitor dissolved in the same buffer. The heat evolved after each injection was obtained from the integral of the calorimetric signal. All data were evaluated with the Origin50 Software package (MicroCal) supplied with the calorimeter. The heat of dilution was subtracted from the observed heat in the binding experiments. The association constants,  $K_a$ , binding enthalpy,  $\Delta H$ , and stoichiometry,  $n$ , were obtained by fitting the data to standard equations for the binding using a model for one set of independent and identical binding sites as implemented in the Origin50 package. The binding entropy  $\Delta S$  and free energy  $\Delta G$  of the binding were calculated from the basic thermodynamic equation,  $\Delta G = -RT \ln K$ , and the Gibbs-Helmholtz equation,  $\Delta G = \Delta H - T\Delta S$ .

**Molecular Modeling**—Docking of the inhibitors to the active site of CALS was performed with AutoDock 3.0 (41). The models were previously protonated by using Chimera (42), and partial charges added as well as solvation parameters were defined by using Antechamber (43). The docking grid was centered on the center of the putative binding site. Fifty dockings were calculated for each inhibitor by using the Lamarckian genetic algorithm (41). All other parameters remained at their default values. The resulting inhibitor binding modes were compared with the hypothetical models built manually by the following procedure: the CALS empty active site was structurally aligned to the structures of the active sites of *M. tuberculosis* LS (MbtLS) complexes with TS13, TS44, and

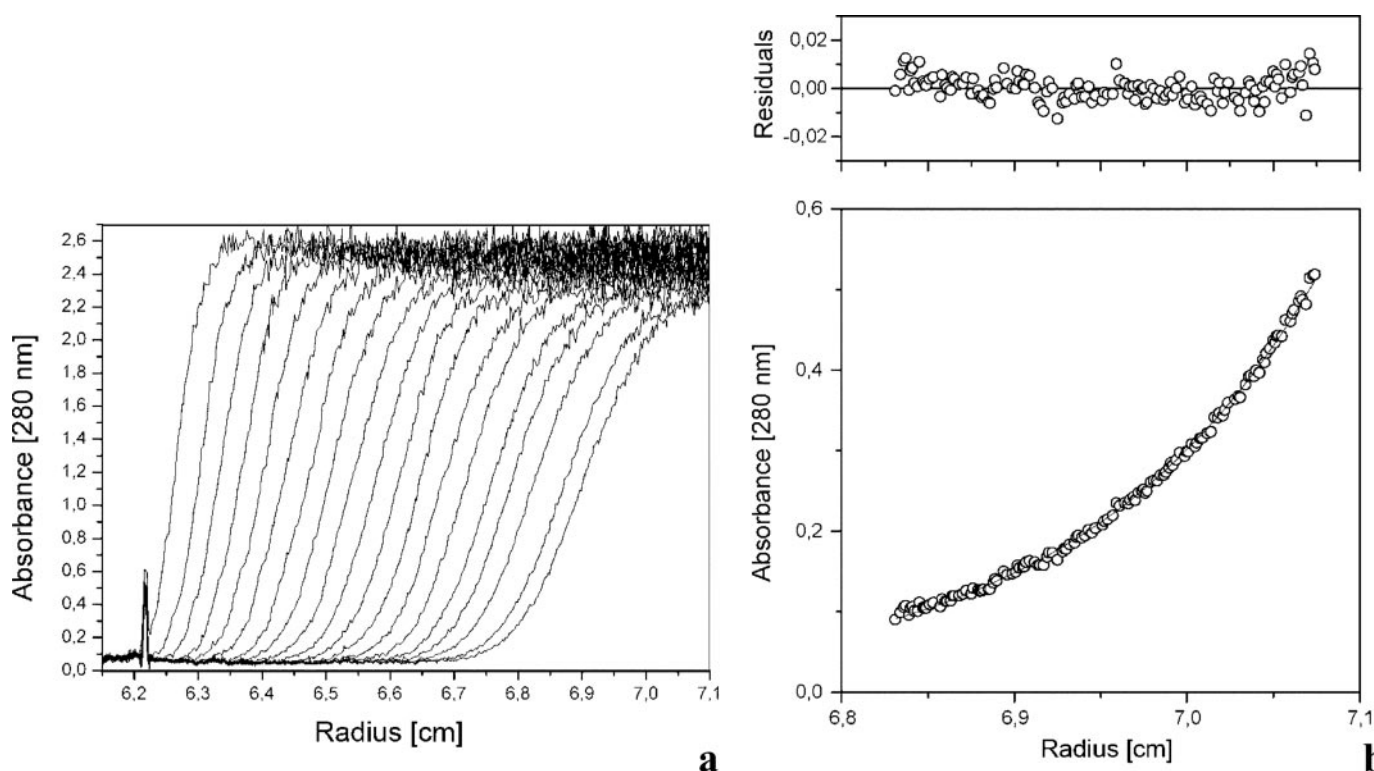


FIGURE 3. Boundary sedimentation (a) and sedimentation equilibrium ultracentrifugation (b) of recombinant lumazine synthase of *C. albicans*.

JC33, respectively. Compound GJ43 was first overlaid with 5-(6-D-ribitylamino-2,4(1*H*,3*H*)-pyrimidinedione-5-yl)-1-pentylphosphonic acid in the active site of LS from *S. cerevisiae*. Then, the obtained hypothetical complex was structurally aligned with the empty CALS pentamer. The structural alignment was performed with the least square option as implemented in O. The resulting structures were subjected to 1000 steps of molecular dynamics calculations followed by 500–700 steps of energy minimization. Molecular dynamics calculations were carried out with the program CNS by using a simulated annealing schedule in Cartesian coordinates at constant temperature 298 K and 0.0005-ps molecular dynamics steps. A constant dielectric constant of 1.0 was applied, and the non-bonded list cut-off was set to 13 Å as default values in CNS. All calculations were performed with fixed main-chain atoms and relaxed side-chain atoms.

## RESULTS AND DISCUSSION

**Cloning, Expression, and Purification**—Sequence homology analysis showed that the hypothetical open reading frame *orf* 19.410.3 of *C. albicans* has an exon-intron structure with one 83-bp intron close to its 5'-end. The resulting hypothetical open reading frame, which predicts a protein of 164 amino acid residues with 72.4% and 37.1% identity to lumazine synthases of *S. cerevisiae* and *A. aeolicus*, respectively (37), was amplified by PCR and was cloned into the expression vector pNCO113. A plasmid harboring the gene under the control of a T5 promoter and a *lac* operator directed the abundant synthesis of a protein with an approximate mass of 18.1 kDa in a recombinant *E. coli* strain. The recombinant protein purified by ion-exchange and gel-permeation chromatography appeared homogeneous as

judged by SDS-PAGE. The enzyme sedimented at an apparent velocity of 5.2 S at 20 °C (Fig. 3*a*). Orthologous lumazine synthases with pentameric structure from the yeasts *S. pombe* and *S. cerevisiae* have been reported to sediment at similar rates of 5.0 and 5.5 S, respectively (44, 45). Sedimentation equilibrium experiments indicated a molecular mass of 91 kDa using an ideal monodisperse model for calculation. The calculated subunit molecular mass of 18,135 Da implicates a pentamer mass of 90.7 kDa in good agreement with the experimental data (Fig. 3*b*). The N-terminal sequence of the recombinant protein was verified by partial Edman degradation affording the sequence motif MAVKGLGEVDQ in perfect agreement with the translated open reading frame.

Enzyme assays confirmed that the protein catalyzes the formation of 6,7-dimethyl-8-ribityllumazine from 5-amino-6-ribitylamino-2,4(1*H*,3*H*)-pyrimidinedione and 3,4-dihydroxy-2-butanone 4-phosphate. Steady-state kinetic analysis afforded a  $v_{\max}$  value of  $10 \mu\text{mol mg}^{-1} \text{h}^{-1}$ .

**Structure of Lumazine Synthase from *C. albicans***—The CALS subunit comprises 164 amino acids and forms a single globular domain folded with  $\alpha/\beta/\alpha$  sandwich topology, which is typical for all other known LSs. The central antiparallel  $\beta$ -sheet has  $\beta_3\beta_2\beta_4\beta_5$  overall topology flanked from both sides by the associated helices  $\alpha_2/\alpha_3$  and  $\alpha_1/\alpha_4/\alpha_5$ , respectively (Fig. 4*a*). All secondary structure elements are separated by short loops, which differ in different LSs. The lengths and conformations of those loops in CALS are more similar to LS from *S. cerevisiae* than to other orthologues. The first 11 residues at the N terminus are disordered in all fifteen subunits. Those residues are disordered in the structures of all known pentameric LSs. The

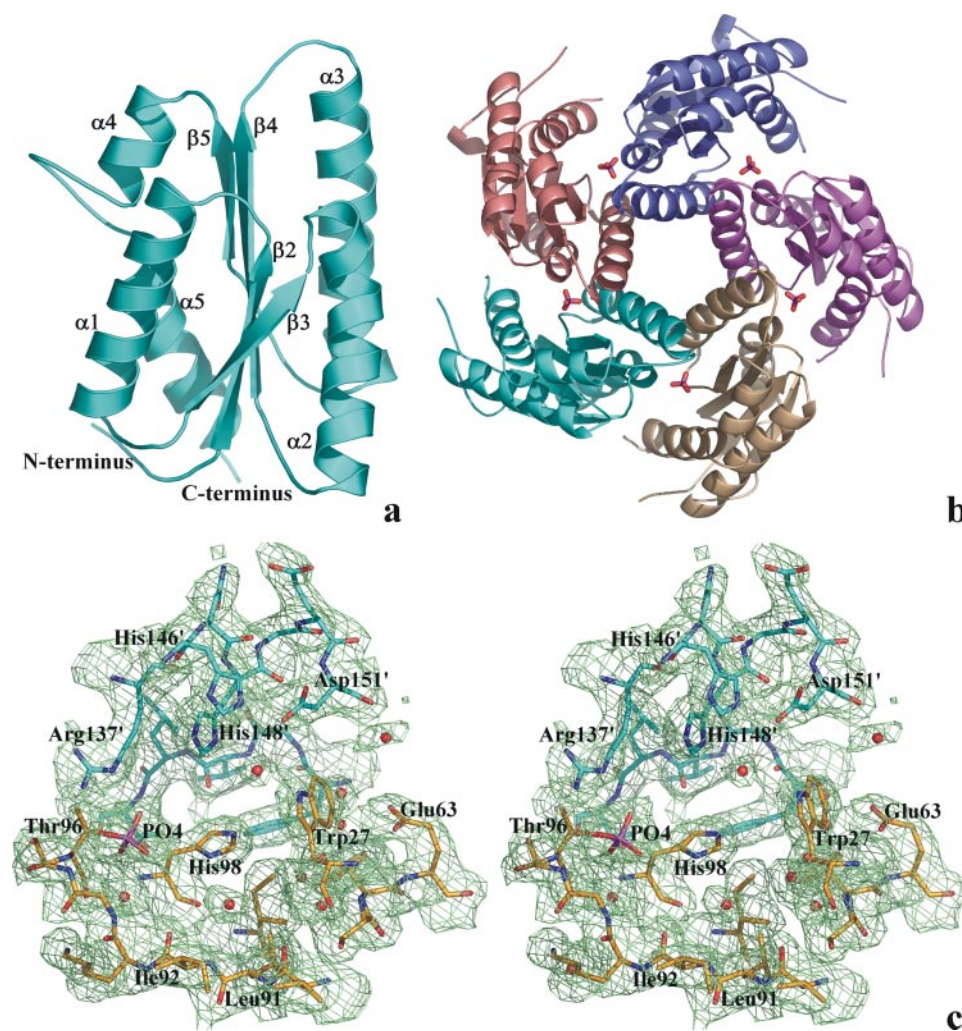


FIGURE 4. **Ribbon representation of lumazine synthase from *C. albicans*.** *a*, secondary structure arrangement of a monomer labeled according to the convention of the *B. subtilis* enzyme (17); *b*, pentameric assembly of the enzyme; five bound inorganic orthophosphate ions are colored red and represented by sticks; *c*, stereodiagrams of the  $2|F_o| - |F_c|$  electron density map ( $\sigma = 2.5$ ) around the active site of *C. albicans* lumazine synthase. Red spheres indicate water molecules. The carbon atoms of the residues of different subunits are shown in green and in yellow. The bound inorganic phosphate ion is shown as a stick model, phosphorus atom colored pink and oxygen atoms colored red. The diagrams in Figs. 4 and 7 are programmed for stereo viewing. Figs. 4, 7, and 8 were generated by PyMOL (W. L. DeLano (2002) PyMOL, DeLano Scientific, San Carlos, CA).

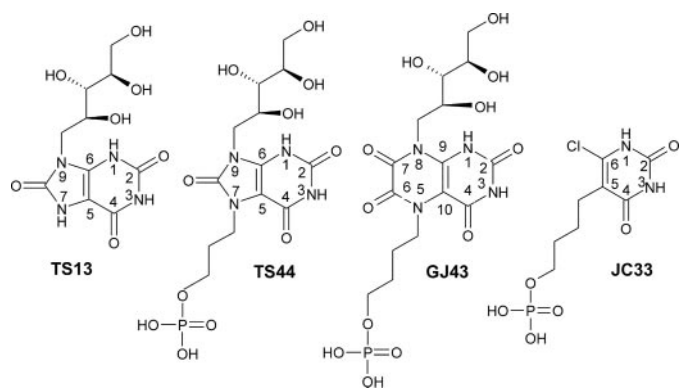


FIGURE 5. **Substrate-analogous inhibitors of lumazine synthase from *C. albicans*.** 1,3,7-Trihydro-9-D-ribityl-2,4,8-purinetrione-7-yl (TS13); 3-(1,3-dihydro-9-D-ribityl-2,4,8-purinetrione-7-yl)propane 1-phosphate (TS44); 4-(6,7(5H,8H)-dioxo-8-D-ribityllumazine-5-yl)butane 1-phosphate (GJ43); and [4-(6-chloro-2,4-dioxo-1,2,3,4-tetrahydropyrimidin-5-yl)butyl] phosphate (JC33).

presence of at least one Pro in the N-terminal sequence was thought to prevent icosahedral capsid formation (11). Up to now, this hypothesis was well confirmed by all known LS structures. Surprisingly, CALS does not have a proline residue in the N terminus, although its sequence is very similar to that in *S. cerevisiae* LS, which contains a proline at position nine (Fig. 2). Nevertheless, in accordance with the structural data and the results of sedimentation equilibrium experiments CALS forms only pentameric assemblies (Fig. 4b). Thus, the driving forces and the structure elements responsible for the formation of pentamers or icosahedrons still remain unclear.

The pentameric assembly of CALS was found to be very similar to all other known LSs (Fig. 4b). Each subunit forms a large contact surface with one neighboring subunit via residues from strands  $\beta_2$ ,  $\beta_3$ , and  $\beta_4$ , helices  $\alpha_2$  and  $\alpha_3$ , and loops connecting  $\beta_3$  to  $\alpha_2$  and  $\beta_4$  to  $\alpha_3$ , and with another neighboring subunit via residues from strand  $\beta_5$ , helices  $\alpha_3$ ,  $\alpha_4$ , and  $\alpha_5$ , and a loop connecting  $\alpha_5$  and  $\beta_3$ . The total surface area buried at the interface of two subunits is  $2527 \text{ \AA}^2$  (calculated with CNS (39)). The total volume of 17 cavities found between the surfaces of two subunits by the program SURFNET (46) resulted in  $2045 \text{ \AA}^3$ . Two connected cavities of  $738$  and  $101 \text{ \AA}^3$ , respectively, form the active site. The residues found in

those two cavities are homologues to the residues in the active sites of previously known LS structures (Fig. 2). Trp-27, known as a most important hydrophobic residue in the substrate binding process, is strictly conserved among pentameric enzymes, but it is replaced by Phe in all known icosahedral structures. The putative 5-amino-6-ribitylamino-2,4-(1*H*,3*H*)-pyrimidinedione (substrate 1) binding site in the CALS structure is occupied by several water molecules, whereas all 15 putative 3,4-dihydroxy-2-butanone 4-phosphate (substrate 2) binding sites in the three pentamers of an asymmetric unit are occupied by a phosphate ion (Fig. 4c). The phosphate ion forms three or four hydrogen bonds with main-chain nitrogen and oxygen atoms of Ser-95 and nitrogen and O $\gamma$ 1 of Thr-95 from one subunit and two hydrogen bonds with Ne and NH $_2$  of Arg-137' from the neighboring subunit. Those contacts with a phosphate ion or the phosphonate group of some inhibitors are well conserved among known LS structures. It is suggested that phos-

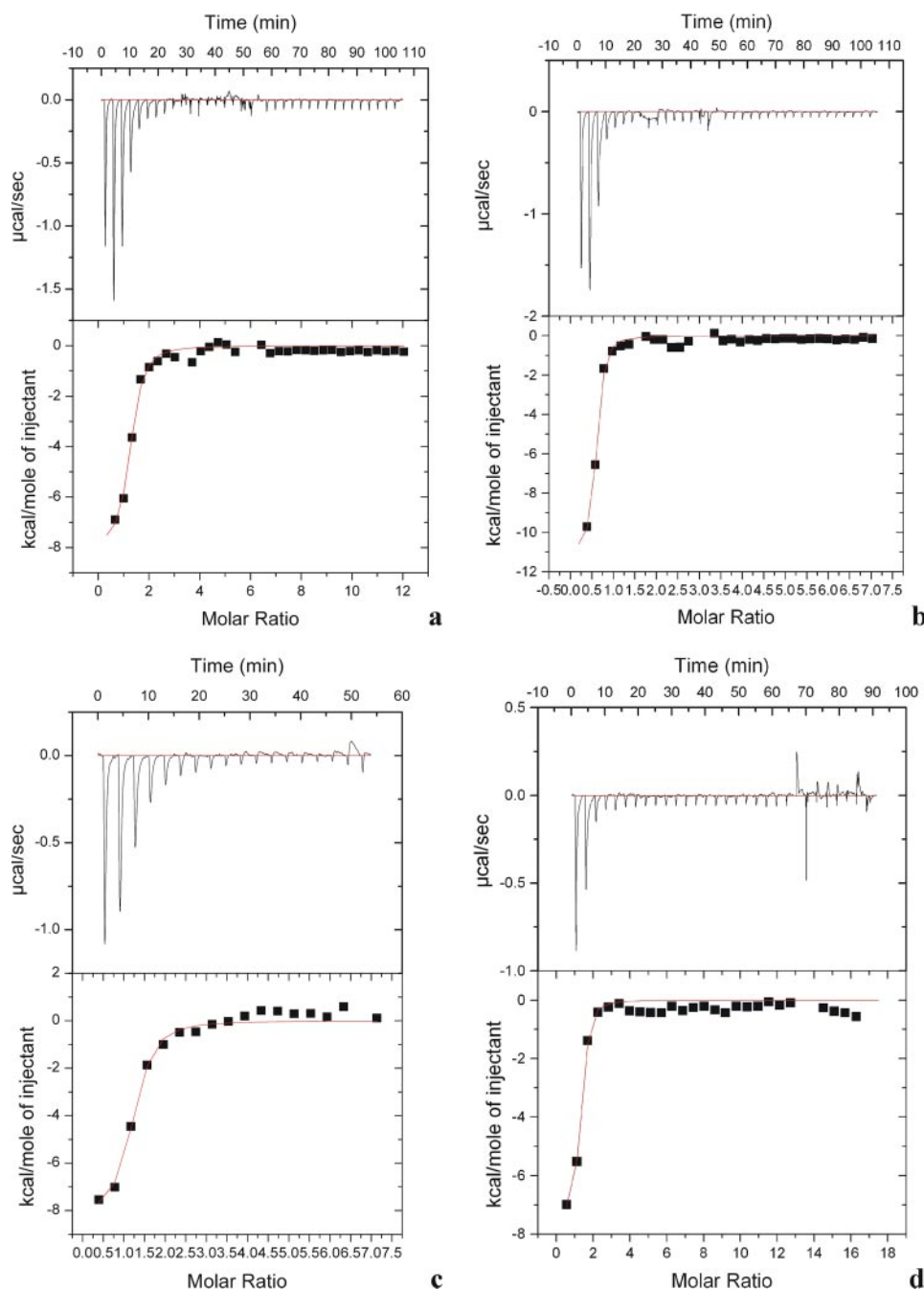


FIGURE 6. Isothermal titration calorimetry data for lumazine synthase from *C. albicans* titrated with 1,3,7-trihydro-9-D-ribityl-2,4,8-purinetrione-7-yl (TS13) (a), 3-(1,3-dihydro-9-D-ribityl-2,4,8-purinetrione-7-yl)butane-1-phosphate (TS44) (b), 4-(6,7(5*H*,8*H*)-dioxo-8-D-ribityl(lumazine-5-yl)butane 1-phosphate (GJ43) (c), and [4-(6-chloro-2,4-dioxo-1,2,3,4-tetrahydropyrimidin-5-yl)butyl] phosphate (JC33) (d). The top panels show the heat changes per injection of inhibitor into enzyme. The bottom panels represent binding isotherms. The red lines present the best results of the fitting data to the chosen model. The experiments were carried out as described under "Experimental Procedures."

phate ions in the pentameric or icosahedral LS structures play a stabilizing role for the pentameric assembly (15). Earlier crystallographic studies of lumazine synthases from various organisms (*B. subtilis*, *S. pombe*, and *A. aeolicus* (10, 18, 47)) all showed orthophosphate ions bound at the site, which is suggested to accept the phosphate moiety of 3,4-dihydroxy-2-butanone 4-phosphate. Probably, phosphate occupies the C4-substrate binding site during catalytically non-productive state. Moreover, all attempts to crystallize any LS in a phosphate-free

environment have ended unsuccessfully or with non-diffracting crystals.

**Binding of Inhibitors**—The successful history of structure determination and inhibitor development on lumazine synthases provided a sound basis to study the interaction of four different inhibitors with the CALS active site. Those inhibitors belonging to four chemical classes differ from each other by their aromatic group usually involved in stacking interactions with the Trp/Phe residue in the active site and by the existence and structure of the functional groups such as the ribityl chain and an alkyl chain bearing a phosphate group. The compounds were synthesized as part of a program to develop LS inhibitors that might act as structural probes of the active site of lumazine synthase. The design of those inhibitors has been based on the structures of both substrates of LS and the putative Schiff base intermediate of the enzymatic reaction (17, 18). The synthesis of all compounds used in our experiments has been published earlier (20, 21). Fig. 5 shows representative chemical structures of the inhibitors. The determinations of the apparent association constants and free energy of the inhibitor-binding reactions were performed by using isothermal titration calorimetry. Analysis of changes in heat accompanying inhibitor binding allowed us to derive binding enthalpy of the processes ( $\Delta H$ ), to estimate stoichiometry ( $n$ ), and association constants ( $K_a$ ), furthermore, to calculate the entropy ( $\Delta S$ ) and free energy ( $\Delta G$ ) of the binding reactions. Fig. 6 shows a typical calorimetric titration of CALS in 50 mM potassium phosphate buffer at pH 7.0 and 30 °C with four different

inhibitors mentioned above. Because our experiments were performed in phosphate buffer, and the phosphate ion has been recognized as a component bound to the LS active site, we would like to emphasize that we in principle are dealing with a ternary binding reaction, involving a phosphate ion, an inhibitor molecule and free enzyme. It has been previously documented that with *M. tuberculosis* lumazine synthase, phosphate increases the apparent  $K_m$  of the substrate 2 and decreases the overall reaction rate (20). This presumably occurs because inor-

**TABLE 3**

Association constants and thermodynamic parameters of binding of different inhibitors to lumazine synthase from *C. albicans*

The entropy of the binding reactions ( $\Delta S$ ) and the free energy change ( $\Delta G$ ) were obtained from the relation  $\Delta G = -RT \ln(K_d) = \Delta H - T\Delta S$ ; the estimated errors of  $\Delta S$  and  $\Delta G$  are obtained from the relations:  $\sigma_{\Delta G} = \frac{R \cdot T}{K_d} \cdot \sigma_{K_d}$  and  $\sigma_{\Delta S} = \sqrt{\left(\frac{d\Delta S}{d\Delta G} \cdot \sigma_{\Delta G}\right)^2 + \left(\frac{d\Delta S}{d\Delta H} \cdot \sigma_{\Delta H}\right)^2} = \sqrt{\left(\frac{-1}{T} \cdot \sigma_{\Delta G}\right)^2 + \left(\frac{1}{T} \cdot \sigma_{\Delta H}\right)^2} = \frac{1}{T} \sqrt{\sigma_{\Delta G}^2 + \sigma_{\Delta H}^2}$ , respectively (54).

	CALS/TS13	CALS/TS44	CALS/GJ43	CALS/JC33
Number of sites, $n$	1.18 ± 0.05	0.95 ± 0.02	1.22 ± 0.04	1.15 ± 0.03
Association constant, $K_d$ , $M^{-1}$	757,800 ± 192,200	3,531,000 ± 932,400	1,632,000 ± 574,200	6,614,000 ± 2,004,000
Binding enthalpy, $\Delta H$ , kcal/mol	-8.60 ± 0.54	-10.01 ± 0.37	-8.97 ± 0.05	-6.98 ± 0.24
Binding entropy, $\Delta S$ , cal/mol · deg	-1.44 ± 0.01	-3.25 ± 0.02	-1.17 ± 0.01	8.16 ± 0.01
Free energy of binding, $\Delta G$ , kcal/mol	-8.17 ± 0.01	-9.12 ± 0.01	-8.63 ± 0.02	-9.38 ± 0.01
Docking binding energy, kcal/mol	-7.4	-11.6	-10.4	-7.0

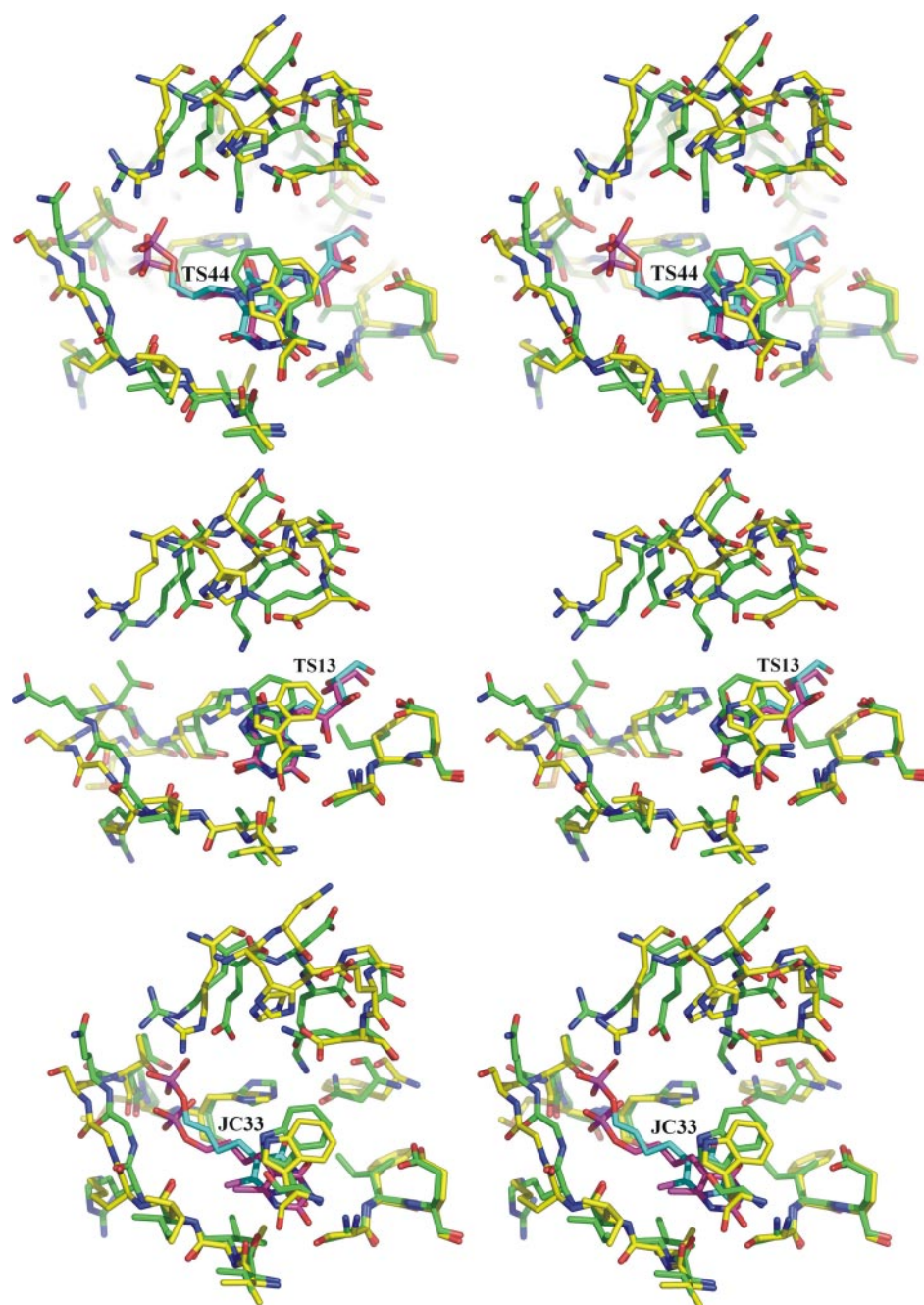


**FIGURE 7. Structural comparison of the active sites of lumazine synthase from *C. albicans* and *M. tuberculosis* with bound inhibitors: 3-(1,3-dihydro-9-D-ribyl-2,4,8-purinetrione-7-yl)butane-1-phosphate (TS44) (a), 1,3,7-trihydro-9-D-ribyl-2,4,8-purinetrione-7-yl (TS13) (b), and [4-(6-chloro-2,4-dioxo-1,2,3,4-tetrahydropyrimidin-5-yl)butyl] phosphate (JC33) (c). The carbon atoms of the residues are shown in yellow and in green for CALS and MbtLS, respectively. The respective inhibitor molecules are shown in magenta for CALS and in cyan for MbtLS. The nitrogen atoms are colored blue, the phosphorus atom is colored pink, and oxygen atoms are colored red.**

ganic phosphate and organic phosphate **2** compete for the same binding site, so it is not unreasonable to assume that inorganic phosphate also competes with phosphate-containing inhibitions in the present case. The association constants and the binding free energies, which we have derived from isothermal titration calorimetry measurements, should thus be considered as “apparent” thermodynamic parameters. During the inhibition reaction this phosphate ion is replaced in a competitive manner by the phosphate group of the inhibitor molecule. Thus, neglecting replacement of water molecules, we have measured the binding free energy of the inhibitor reduced by the free energy contribution of phosphate binding at its binding place.

Fitting binding isotherms of all four inhibitors was achieved with a model using a “single set of identical sites” assuming that each of the active sites in the pentameric assembly is occupied by one inhibitor molecule. The thermodynamic characteristics are shown in Table 3. Binding of all four inhibitors is exothermic with negative changes in binding enthalpy. The apparent association constants are in the range between  $6.61 \times 10^6 M^{-1}$  for the CALS·JC33 complex and  $7.58 \times 10^5 M^{-1}$  for the CALS·TS13 complex, respectively. The weakest affinity is shown by the TS13 compound, which is lacking the phosphate-bearing aliphatic chain. This finding is in good agreement with a previously shown tendency of increased affinity of inhibitors obtained by attaching the phosphate-bearing aliphatic chain to the hydrophobic moiety of the inhibitor

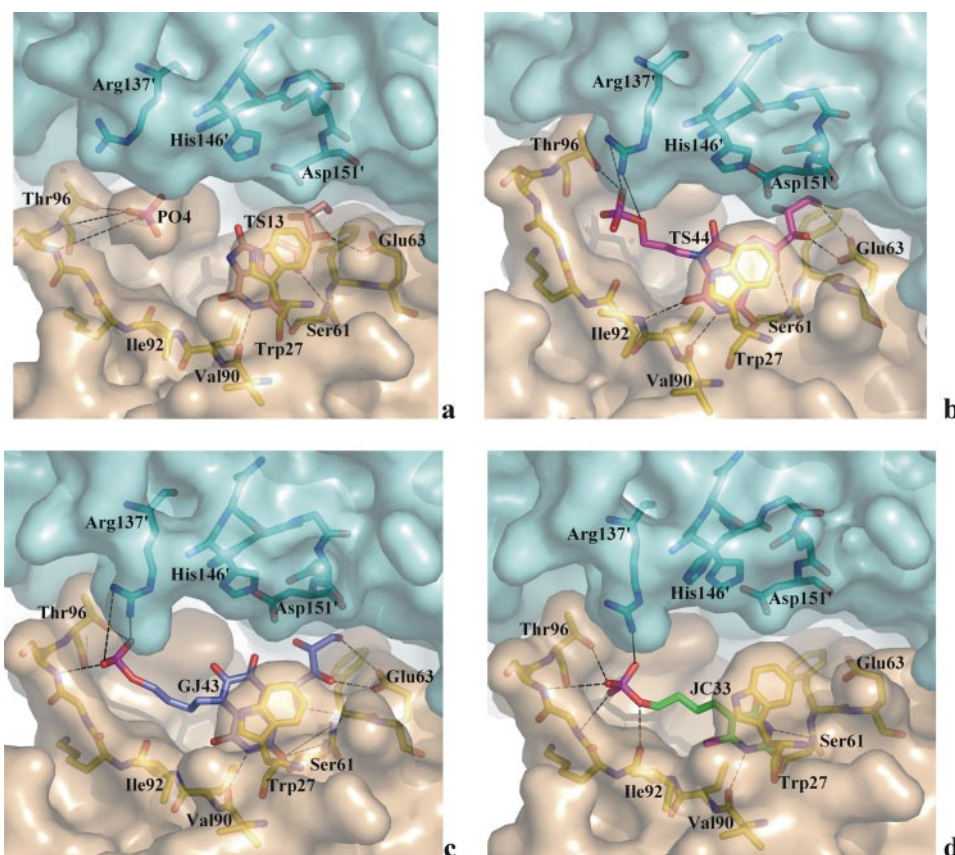


**FIGURE 8.** Surface representation of the results of docking of the inhibitors 1,3,7-trihydro-9-D-ribityl-2,4,8-purinetrione-7-yl (TS13) (a), 3-(1,3-dihydro-9-D-ribityl-2,4,8-purinetrione-7-yl)butane-1-phosphate (TS44) (b), 4-(6,7(5H,8H)-dioxo-8-D-ribityllumazine-5-yl)butane-1-phosphate (GJ43) (c), and [4-(6-chloro-2,4-dioxo-1,2,3,4-tetrahydropyrimidin-5-yl)butyl] phosphate (JC33) (d) to the putative active site of lumazine synthase from *C. albicans*. The accessible surfaces were calculated with a water probe radius of 1.4 Å. Two adjacent subunits, constituting the active site, are shown in different colors (cyan and gold); the inhibitor molecules are shown in orange, magenta, blue, and green, respectively. The dashed lines represent the putative interactions between inhibitor and enzyme molecules.

(20, 21, 48). It has been shown that the purinetrione ring system with an attached C5-phosphate side chain resulted in a less potent inhibitor of *B. subtilis* LS (20); however, it revealed a high inhibition potential for the pentameric enzyme from *M. tuberculosis* (12, 20, 49). The present investigation of binding processes has shown that the values of the association constants of those inhibitors to CALS are in a similar range compared with those for *M. tuberculosis* LS. CALS inhibitor complexes access a broader range of  $\Delta H$  values than  $\Delta G$  values, although they are always favorable at 293 K (Table 3). This may be a result of the “enthalpy-entropy compensation effect,” which is believed to be a consequence of protein-ligand interactions mediated by multiple weak interactions that also involve water molecules (50, 51). The negative enthalpy changes associated with the binding indicate that favorable polar and hydrophobic interactions are generated between the bound inhibitors and the amino acid residues in the active site. The thermodynamic characteristics of the binding of TS13, TS44, and GJ43 indicate that the association processes are favored enthalpically but disfavored entropically. The negative entropy contribution ( $-T\Delta S = -2.39$  kcal/mol) found for the binding of JC33 contributes in a favorable way to the free energy of binding. This may be due to the lack of interaction between the ribityl chain

and both protein subunits forming the active site, and by weaker hydrophobic interactions of the pyrimidine ring with the aromatic group of Trp-27. This compound demonstrated even a slightly higher association constant than the other three inhibitors (the association constant,  $K_a = 6.61 \times 10^6 \text{ M}^{-1}$ , is the largest among the studied reactions). Moreover, because the space in which the ribityl chain is supposed to be embedded is occupied by several water molecules in the empty active site, the lack of the ribityl chain in JC33 makes the replacement of those water molecules with hydroxyl groups of the ribityl chain unnecessary.

**Structure-based Modeling of the Inhibitor Binding Mode**—A comparison of the crystallographic structures of pentameric lumazine synthase assemblies from different bacteria has revealed that these structures are very similar and that no major conformational changes occur upon inhibitor binding. Notable conformational changes, however, were observed for Phe-22, His-88, Arg-127, and Glu-126 upon inhibitor binding in icosahedral *A. aeolicus* LS (18). According to these facts we have undertaken docking studies of inhibitors to the active

site and we present in this report the hypothetical binding modes for complexes of CALS with all four inhibitors described above. Calculations carried out with Autodock for compound TS44 revealed all obtained 50 models in the same position inside the active site corresponding to the binding mode of this compound in the MbtLS/TS44 structure (12) (Fig. 7a). The position of the phosphate moiety was slightly shifted from model to model. Docking results of the other inhibitors were less obvious. For each of the ligands several clusters of positions were found. For example, the compounds TS13 and JC33 were found in an “upside-down” position in the active site or in positions in which the ribityl chain occupied the phosphate binding site (TS13) or the aliphatic chain was embedded at the subunit interface, involving a rotation (“rotated” position) of the inhibitor (JC33). Similar positions were also observed among GJ43 docking results. Several binding modes of GJ43 were found rather far away from the active site, and several modes were found in close proximity of the active site but not well positioned in the cavity. A most logical explanation for these results can be found from a comparison of the present inhibitor structures with the intermediates of the enzymatic reactions, which are mimicked by those inhibitors. Compound TS44 is most similar to one of the suggested intermediates (18). Compound

**TS13** lacks the aliphatic connection to the phosphate moiety, and compound **JC33** lacks the ribityl chain and has a rather small aromatic system. Both compounds are small enough to diffuse into the active site easily and to fit either in the upside-down or in the rotated position. In both cases the number of possible contacts is reduced in comparison to the most likely binding mode. Compound **GJ43** is a bit more bulky than **TS44** and any of the suggested intermediates, because it has an aliphatic chain that is one carbon atom longer. Furthermore, its aromatic ring system is somewhat more extended than the purintrione system. Thus, this compound can apparently have steric problems when entering the active site cavity. Clusters corresponding to the position and orientation expected from homologous structures were suggested to be a correct binding model. The best docking results revealed a rather good agreement with the inhibitor positions in the known MbtLS-inhibitor complex structures considering the existing differences in the amino acid sequences in between CALS and MbtLS (see Fig. 7). The binding energy estimated during the docking procedure of compound **TS44** was found to be  $-11.67$  kcal/mol, whereas the averaged corresponding energies for the best clusters of **TS13**, **GJ43**, and **JC33** were  $-7.43$ ,  $-10.42$ , and  $-7.06$  kcal/mol, respectively. Fig. 8 represents the resulting binding models derived from manual docking. As expected, the calculated structures showed the aromatic groups of the inhibitors in a stabilizing arrangement with the indole ring of Trp-27. The energy minimization procedure turned the indole ring of Trp-27 to a parallel conformation with respect to the plane of the aromatic groups of all inhibitors, whereas the indole group in the empty structure assumed different conformations in different subunits. This conformational change of the side chain of Trp-27 is in good agreement with the conformations of the aromatic groups of tryptophan or phenylalanine found in the structures of different LSs inhibitor complexes (9, 10, 12, 18, 49, 52, 53). The main-chain contacts, found conserved in all orthologous complexes, remained unchanged in the binding models of all inhibitors. The carbonyl oxygen O2 and nitrogen N3 from the aromatic moiety of all four ligands showed hydrogen bond contacts with the main-chain nitrogen and the side-chain oxygen of Ser-61, as well as with the main-chain oxygens of Val-90 and Leu-91. There is also a free space for water molecules mediating the contacts between inhibitor and protein molecules that are known to exist in the structures of different LSs. The phosphate moiety of the ligands is extensively hydrogen-bonded to the side-chain nitrogens of Arg-137, as well as the backbone nitrogens of Ala-95 and Thr-96 and the side-chain hydroxyl of Thr-96. Compounds **GJ43** and **JC33**, containing a C4-alkyl phosphate chain, showed more contacts of the phosphate moiety in comparison with **TS44**, which has only three carbon atoms in that chain. The position of the phosphate moiety in the complex with **GJ43** and **JC33** is superimposed with the position of the phosphate ion found in the empty structure. In comparison with that position of the phosphate ion, the phosphate moiety of **TS44** is shifted to the center of the active site cavity due to the shortened aliphatic chain. The ribityl chains of **TS13**, **TS44**, and **GJ43** are embedded in the interface of two subunits and form hydrogen bond contacts with the side-chain oxygens of Glu-63 and the main-chain nitrogen of

Ser-61. The volume occupied by the ligand molecules was calculated with SURFNET and resulted in the values of 216, 307, 344, and 211 Å<sup>3</sup> for **TS13**, **TS44**, **GJ43**, and **JC33**, respectively. Comparison of the total volume of the active site cavity (840 Å<sup>3</sup>) with the values mentioned above points to a quite large space that might be occupied by water molecules during the binding process.

**Conclusion**—The current work has shown that the combination of structural analysis, thermodynamic inhibition data, docking, and knowledge of mechanistic details provides a valuable tool for structure-based drug design. The structure of lumazine synthase from *C. albicans* reveals the specific features of this protein in comparison with the other family members. Complementary structural and biochemical work has provided a basis for further investigation and development of new specific anti-fungal agents directed against *C. albicans* infections in immunocompromised patients.

**Acknowledgments**—We gratefully acknowledge the access to synchrotron radiation facilities at the EMBL Outstation in Hamburg and thank Dr. A. Popov for the help at the beamline. We also thank Guangyi Jin, Jinhua Chen, and Thota Sambaiah for providing us with inhibitor compounds.

## REFERENCES

- Schaberg, D. R., Culver, D. H., and Gaynes, R. P. (1991) *Am. J. Med.* **91**, S71–S75
- d'Enfert, C., Goyard, S., Rodriguez-Arnaveilhe, S., Frangeul, L., Jones, L., Tekaiia, F., Bader, O., Albrecht, A., Castillo, L., Dominguez, A., Ernst, J. F., Fradin, C., Gaillardin, C., Garcia-Sanchez, S., de Groot, P., Hube, B., Klis, F. M., Krishnamurthy, S., Kunze, D., Lopez, M. C., Mavor, A., Martin, N., Moszer, I., Onesime, D., Perez Martin, J., Sentandreu, R., Valentin, E., and Brown, A. J. (2005) *Nucleic Acids Res.* **33(Database issue)**, D353–D357
- Graybill, J. R. (1996) *Clin. Infect. Dis.* **22**, Suppl. 2, S166–S178
- Warnock, D. W. (1995) *J. Antimicrob. Chemother.* **36**, Suppl. B, 73–90
- Shavlovsky, G. M., Teslyar, G. E., and Strugovshchikova, L. P. (1982) *Mikrobiologiya* **51**, 986–992
- Shavlovsky, G. M., Sibirny, A. A., Kshanovskaya, B. V., Koltun, L. V., and Logvinenko, E. M. (1979) *Genetika* **15**, 1561–1568
- Oltmanns, O., Bacher, A., Lingens, F., and Zimmermann, F. K. (1969) *Mol. Gen. Genet.* **105**, 306–313
- Echt, S., Bauer, S., Steinbacher, S., Huber, R., Bacher, A., and Fischer, M. (2004) *J. Mol. Biol.* **341**, 1085–1096
- Meining, W., Mörtl, S., Fischer, M., Cushman, M., Bacher, A., and Ladenstein, R. (2000) *J. Mol. Biol.* **299**, 181–197
- Gerhardt, S., Haase, I., Steinbacher, S., Kaiser, J. T., Cushman, M., Bacher, A., Huber, R., and Fischer, M. (2002) *J. Mol. Biol.* **318**, 1317–1329
- Persson, K., Schneider, G., Jordan, D. B., Viitanen, P. V., and Sandalova, T. (1999) *Protein Sci.* **8**, 2355–2365
- Morgunova, E., Meining, W., Cushman, M., Illarionov, B., Haase, I., Jin, G., Bacher, A., Cushman, M., Fischer, M., and Ladenstein, R. (2005) *Biochemistry* **44**, 2746–2758
- Braden, B. C., Velikovskiy, C. A., Cauerhff, A. A., Polikarpov, I., and Goldbaum, F. A. (2000) *J. Mol. Biol.* **297**, 1031–1036
- Zylberman, V., Craig, P. O., Klinke, S., Braden, B. C., Cauerhff, A., and Goldbaum, F. A. (2004) *J. Biol. Chem.* **279**, 8093–8101
- Bacher, A., Ludwig, H. C., Schnepfle, H., and Ben-Shaul, Y. (1986) *J. Mol. Biol.* **187**, 75–86
- Zhang, X., Meining, W., Fischer, M., Bacher, A., and Ladenstein, R. (2001) *J. Mol. Biol.* **306**, 1099–1114
- Kis, K., Volk, R., and Bacher, A. (1995) *Biochemistry* **34**, 2883–2892
- Zhang, X., Meining, W., Cushman, M., Haase, I., Fischer, M., Bacher, A., and Ladenstein, R. (2003) *J. Mol. Biol.* **328**, 167–182

19. Ritsert, K., Huber, R., Turk, D., Ladenstein, R., Schmidt-Bäse, K., and Bacher, A. (1995) *J. Mol. Biol.* **253**, 151–167
20. Cushman, M., Sambaiah, T., Jin, G., Illarionov, B., Fischer, M., and Bacher, A. (2004) *J. Org. Chem.* **69**, 601–612
21. Cushman, M., Jin, G., Sambaiah, T., Illarionov, B., Fischer, M., Ladenstein, R., and Bacher, A. (2005) *J. Org. Chem.* **70**, 9092
22. Cresswell, R. M., Neilson, T., and Wood, H. C. S. (1960) *J. Chem. Soc.* **1960**, 4776–4779
23. Sedlmaier, H., Müller, F., Keller, P. J., and Bacher, A. (1987) *Z. Naturforsch. [C]* **42**, 425–429
24. Bacher, A., Neuberger, G., and Volk, R. (1986) *Chem. Biol. Clin. Aspects* **8**, 227–230
25. Richter, G., Kelly, M., Krieger, C., Yu, Y., Bermel, W., Karlsson, G., Bacher, A., and Oschkinat, H. (1999) *Eur. J. Biochem.* **261**, 57–65
26. Kis, K., and Bacher, A. (1995) *J. Biol. Chem.* **270**, 16788–16795
27. Bullock, W. O., Fernandez, J. M., and Shout, J. M. (1987) *BioTechniques* **5**, 376–380
28. Stüber, D., Matile, H., and Garotta, G. (1990) in *Immunological Methods* (Lefkowitz, I., and Pernis, B. eds) pp. 121–125, Academic Press, New York
29. Laue, T. M., Shah, B. D., Ridgeway, T. M., and Pelletier, S. L. (1992) *Computer-aided Interpretation of Analytical Sedimentation Data for Proteins*, Royal Society of Chemistry, Cambridge
30. Sanger, F., Nicklen, S., and Coulson, A. R. (1977) *Proc. Natl. Acad. Sci. U. S. A.* **74**, 5463–5467
31. Read, S. M., and Northcote, D. H. (1981) *Anal. Biochem.* **116**, 53–64
32. Laemmli, U. K. (1970) *Nature* **227**, 680–685
33. Bourenkov, G. P., and Popov, A. N. (2006) *Acta Crystallogr. Sect. D Biol. Crystallogr.* **62**, 58–64
34. Otwinowski, Z., and Minor, W. (1997) *Methods Enzymol.* **276**, 307–326
35. Lu, G. (1999) *J. App. Crystallogr.* **32**, 375–376
36. CCP4 (1994) *Acta Crystallogr. Sect. D Biol. Crystallogr.* **50**, 760–763
37. Thompson, J. D., Higgins, D. G., and Gibson, T. J. (1994) *Nucleic Acids Res.* **22**, 4673–4680
38. Matthews, B. W. (1968) *J. Mol. Biol.* **33**, 491–497
39. Brünger, A. T., Adams, P. D., Clore, G. M., DeLano, W. L., Gros, P., Grosse-Kunstleve, R. W., Jiang, J.-S., Kuszewski, J., Nilges, M., Pannu, N. S., Read, R. J., Rice, L. M., Simonson, T., and Warren, G. L. (1998) *Acta Crystallogr. Sect. D Biol. Crystallogr.* **54**, 905–921
40. Jones, A. T., Zou, J. Y., Cowtan, J. Y., and Kjeldgaard, M. (1991) *Acta Crystallogr. Sect. A* **47**, 110–119
41. Morris, G. M., Goodsell, D. S., Halliday, R. S., Huey, R., Hart, W. E., Belew, R. K., and Olson, A. J. (1998) *J. Comput. Chem.* **19**, 1639–1662
42. Pettersen, E. F., Goddard, T. D., Huang, C. C., Couch, G. S., Greenblatt, D. M., Meng, E. C., and Ferrin, T. E. (2004) *J. Comput. Chem.* **25**, 1605–1612
43. Wang, J., Wang, W., Kollman, P. A., and Case, D. A. (2006) *J. Mol. Graph Model* **25**, 247–260
44. Mörtl, S., Fischer, M., Richter, G., Tack, J., Weinkauff, S., and Bacher, A. (1996) *J. Biol. Chem.* **271**, 33201–33207
45. Fischer, M., Haase, I., Feicht, R., Richter, G., Gerhardt, S., Changeux, J. P., Huber, R., and Bacher, A. (2002) *Eur. J. Biochem.* **269**, 519–526
46. Laskowski, R. A. (1995) *J. Mol. Graphics* **13**, 323–330, 307–328
47. Schott, K., Kellermann, J., Lottspeich, F., and Bacher, A. (1990) *J. Biol. Chem.* **265**, 4204–4209
48. Cushman, M., Mihalic, J. T., Kis, K., and Bacher, A. (1999) *J. Org. Chem.* **64**, 3838–3845
49. Morgunova, E., Illarionov, B., Sambaiah, T., Haase, I., Bacher, A., Cushman, M., Fischer, M., and Ladenstein, R. (2006) *FEBS J.* **273**, 4790–4804
50. Dunitz, J. D. (1995) *Chem. Biol.* **2**, 709–712
51. Baker, B. M., and Murphy, K. P. (1996) *Biophys. J.* **71**, 2049–2055
52. Ladenstein, R., Schneider, M., Huber, R., Bartunik, H. D., Wilson, K., Schott, K., and Bacher, A. (1988) *J. Mol. Biol.* **203**, 1045–1070
53. Klinke, S., Zylberman, V., Vega, D. R., Guimaraes, B. G., Braden, B. C., and Goldbaum, F. A. (2005) *J. Mol. Biol.* **353**, 124–137
54. Taylor, J. R. (1997) *An Introduction to Error Analysis: The Study of Uncertainties in Physical Measurements*, Second Ed., p. 75, University Science Books, Sausalito, CA